Available online at www.sciencedirect.com
SCIENCE DIRECT®
Journal of Nuclear Materials 348 (2006) 133–147
journal of nuclear materials
www.elsevier.com/locate/jnucmat

The electrochemistry of zirconium in aqueous solutions at elevated temperatures and pressures

Yingzi Chen [a], Mirna Urquidi-Macdonald [b], Digby D. Macdonald [a,*]

[a] Center for Electrochemical Science and Technology, Department of Materials Science and Engineering, Pennsylvania State University, 201 Steidle Building, University Park, PA 16802, USA
[b] Department of Engineering Science and Mechanics, Pennsylvania State University, University Park, PA 16802, USA

Received 22 July 2005; accepted 6 September 2005

Abstract

The electrochemistry of zirconium has been explored in borate buffer solution of pH = 6.94 at 250 °C with and without hydrogen by measuring the current, impedance, and capacitance as a function of potential. Data are interpreted in terms of modified point defect models (PDM) that recognize the existence of a thick oxide outer layer over a thin barrier layer. From thermodynamic analysis, it is postulated that a hydride barrier layer forms under PWR coolant conditions whereas an oxide barrier layer forms under BWR primary coolant conditions. Thus, the introduction of hydrogen into the solution lowers the corrosion potential of zirconium to the extent that the formation of ZrH_2 is predicted to be spontaneous rather than the ZrO_2. Mott–Schottky analysis shows that the passive film formed on zirconium is *n*-type, which is consistent with the PDM, corresponding to a preponderance of oxygen/hydrogen vacancies and/or zirconium interstitials in the barrier layer.

PACS: 82.45.Bb; 84.37.+q; 81.65.Rv; 82.45.Cc

1. Introduction

Zirconium and its alloys have been studied extensively [1–19] in response to their application in thermal nuclear reactors of separating the coolant water from the nuclear fuel. They are used because of their low thermal neutron capture cross-section and excellent corrosion resistance. The principal threat to the integrity of the zirconium alloy fuel cladding (Zircaloy) is oxidation/corrosion and hydriding, leading to more-or-less uniform thinning and, in some instances, to localized corrosion in the form of nodular attack and/or hydriding. Failure leads to the release of fission products into the coolant, which in turn contributes to the radiation exposure costs of operating the system. Extensive fuel failures may require shutdown, which results in the unit being unavailable for normal operation. Thus, strong operational and economic reasons exist for enhancing fuel cladding reliability and any successful program to achieve this goal requires a detailed knowledge of the electrochemistry and corrosion

* Corresponding author. Tel.: +1 814 863 7772; fax: +1 814 863 4718.
E-mail address: ddm2@psu.edu (D.D. Macdonald).

0022-3115/$ - see front matter © 2005 Elsevier B.V. All rights reserved.
doi:10.1016/j.jnucmat.2005.09.014

behavior of zirconium and its alloys. Initial work on investigating the electrochemistry and passivity of zirconium and its alloys was that by Gunterschultze and Betz [20] in 1931 (well before the advent of nuclear reactors), who described the passive behavior of a number of valve metals. With the development of nuclear power reactors and in particular high burn-up fuels, the corrosion of zirconium alloys in high-temperature aqueous solutions has become a matter of considerable interest to the electrical utility industry [21].

Most early investigations of the corrosion behavior of zirconium and its alloys (e.g., Zircaloys) in aqueous solutions focused on either ex situ or in situ studies at or near ambient temperature. Ex situ studies necessarily require interruption of the corrosion experiment, which introduces considerable uncertainty into the subsequent analysis. For this reason, emphasis was quickly focused on devising in situ analytical techniques (e.g., in situ spectroscopic methods), so that the corrosion processes could be examined under actual operating conditions. Most of these techniques are electrochemical in nature and have begun to yield a great deal of valuable information, provided that the data are properly interpreted. Of course, various electron microscopy techniques, such as SEM, TEM, and STEM, which have provided much structural information of the passive film [22–25], are necessarily ex situ by their very nature and always will be so, although various X-Ray diffraction and scattering techniques (e.g., XANES, EXAFS, SEXAFS) using intense light sources (synchrotron radiation) may provide the in situ capability, even under elevated temperature and pressure conditions.

This paper focuses on in situ electrochemical studies of zirconium in high temperature aqueous solutions; no attempt has been made to study the corrosion behavior gravimetrically, as that has been adequately explored by others [21]. Potentiostatic polarization, potentiodynamic polarization, and electrochemical impedance spectroscopy (EIS) are the principal techniques used, with the latter also being employed for determining passive film thickness and for carrying out Mott–Schottky analyses. Durand-Keklikian et al. [27,28] reported both in situ and ex situ impedance studies on oxidized zirconium alloys, including in situ 'contact impedance' measurement in steam (supercritical water) at 500 °C and 650 bar under conditions that lead to nodular attack. The ex situ impedance data were consistent with nodular attack resulting in the development of a large number of parallel conductive paths in the normally resistive oxide. Later, Hettiarachi et al. [29] performed potentiodynamic and impedance studies to characterize the electrochemical corrosion behavior of Zircaloy-2 and Zircaloy-4 at 289 °C in 8 ppm $NaNO_3$ solution under open circuit potential conditions. The Zircaloys display stable passivity in the presence of high dissolved oxygen contents and the active-to-passive transition, which is not observed at high oxygen concentrations, reappears at lower oxygen contents, by virtue of the negative shift in the corrosion potential. Impedance data for the passive films formed on the two Zircaloys confirmed the greater corrosion resistance of Zr-2 over Zr-4. Schefold et al. [30] carried out long term, in situ impedance measurement on Zr and Zr-4 in pressurized aqueous solutions at 633 K (360 °C), also under open circuit potential conditions. Cyclical corrosion behavior was demonstrated in their long term corrosion tests, which implies two rate determining elements, the in-cycle growth and the rupture thickness of the protective layer. Nagy et al. [31–33] published a series of papers on the oxidation of Zr–1%Nb under simulated VVER–PWR primary coolant conditions at temperatures up to 290 °C using a two electrode arrangement. A -$CPE_{ox}\|R_{ox}$- element was incorporated into the equivalent electrical circuit to explain the impedance spectroscopy data measured under open circuit potential conditions. They found both the CPE_{ox} coefficient and the parallel resistance R_{ox} to be thickness dependent and they postulated that the temperature dependence of R_{ox} indicates that the oxide layer has semiconductor properties.

As noted above, in this contribution the electrochemistry of zirconium has been explored in situ in 0.1 M $B(OH)_3 + 0.001$ M LiOH solution (pH = 6.94 at 250 °C) with and without added hydrogen to simulate the water chemistries of the coolant circuits in pressurized water reactors (PWRs) and boiling water reactors (BWRs). Potentiostatic polarization, potentiodynamic polarization, and electrochemical impedance spectroscopic (EIS) techniques were used, with the latter also being employed for determining passive film thickness and for carrying out Mott–Schottky analyses. The lower temperature than that found in reactor coolant circuits (288 °C for BWRs and 360 °C for PWRs) was dictated by the need to use PTFE in the electrochemical cell and the use of the boric acid/lithium hydroxide solution for the BWR case was dictated by the need to maintain constant pH and significant conductiv-

ity. The primary objective of this initial work on pure zirconium was to develop and demonstrate the experimental techniques and to provide a database for the pure metal against which the alloys may be compared in subsequent work. We have employed the point defect model (PDM) [34,35], which provides an atomistic description of the growth and breakdown of oxide and hydride [34] barrier layers in terms of the generation and annihilation of crystallographic defects at the interfaces of the film and their transport under the influence of an electrical potential gradient within the oxide (or hydride) phase, to interpret the experimental data. While a complete interpretation of all of the experimental data (particularly the EIS data) will be reported at a later date, it is worth noting here that the PDM has been considerably modified by the incorporation of the outer, porous oxide layer and the formation of a defective hydride (ZrH_{2-x}) barrier layer in the case of hydrogenated solutions and a defective oxide (ZrO_{2-x}) layer in the case of non-hydrogenated solutions [36]. As demonstrated elsewhere [36], the relative values of the corrosion potentials in the two environments and the equilibrium potential for the Zr/ZrH_2 and Zr/ZrO_2 couples at the elevated temperatures of interest are such that the formation of a hydride barrier layer is thermodynamically spontaneous under PWR coolant conditions whereas the formation of an oxide barrier layer is spontaneous under BWR primary coolant conditions.

2. The electrochemical thermodynamics of reactor cores

Before proceeding further, it is necessary to discuss briefly the electrochemical thermodynamics of the fuel cladding in BWRs and PWRs. In order to do so, the equilibrium properties of the Zr/ZrO_2, ZrH_2/Zr, and ZrH_2/ZrO_2 couples need to be calculated, where the reduced species is on the left side and the oxidized species is on the right side. Following the Stockholm convention, we write all half cell reactions in the reduction sense as

$$ZrO_2 + 4H^+ + 4e^- = Zr + 2H_2O \quad (1)$$

$$Zr + 2H^+ + 2e^- = ZrH_2 \quad (2)$$

and

$$ZrO_2 + 6H^+ + 6e^- = ZrH_2 + 2H_2O \quad (3)$$

to yield the cell reactions as

$$ZrO_2 + 2H_2 = Zr + 2H_2O \quad (4)$$

$$Zr + H_2 = ZrH_2 \quad (5)$$

and

$$ZrO_2 + 3H_2 = ZrH_2 + 2H_2O \quad (6)$$

The standard potential is then given by $E^0 = -\Delta G^0_R/nF$, where ΔG^0_R is the change in standard Gibbs energy for Reactions (4)–(6), n is the number of electrons involved in the half cell reaction, and F is Faraday's constant (96 487 C/equiv.). Calculation of the standard potentials at temperatures up to the maximum core temperature of the reactor type of interest was carried out using the HSC Chemistry software [37]. The half cell reactions can be written in general form as

$$aA + xH^+ + ne^- = bB + cH_2O \quad (7)$$

from which we derive the Nernst equation as

$$E^e = E^0 - \frac{2.303RT}{F}\left(\frac{b}{n}\right)\log(a_B) + \frac{2.303RT}{F}\left(\frac{a}{n}\right)\log(a_A) - \frac{2.303RT}{F}\left(\frac{c}{n}\right)\log(a_{H_2O}) - \frac{2.303RT}{F}\left(\frac{x}{n}\right)pH, \quad (8)$$

where E^e is the equilibrium potential, a_i is the activity of species i, R is the universal gas constant ($R = 8.3124$ J/K mol), and $pH = -\log(a_{H^+})$. Because the reactants and products are solids, their activities may be set to one and, since the solutions are reasonably dilute, $a_{H_2O} = 1$. Thus, Eq. (8) reduces to the much simpler form

$$E = E^0 - \frac{2.303RT}{F}\left(\frac{x}{n}\right)pH, \quad (9)$$

where x is the stoichiometric coefficient of H^+ in the half cell reactions, Eqs. (1)–(3).

That the electrochemical conditions in the cores of BWRs and PWRs differ substantially is demonstrated by Fig. 1, in which is plotted the equilibrium potentials for the Zr/ZrO_2 and ZrH_2/Zr couples as a function of temperature [36]. Also plotted are the ECP (corrosion potential) values for the fuel channels in the two types of reactors, as determined by thermohydraulic/radiolysis/electrochemical modeling in this laboratory. The reader will note that the formation of ZrO_2 is an oxidation process ($Zr + 2H_2O \rightarrow ZrO_2 + 4H^+ + 4e^-$), whereas the

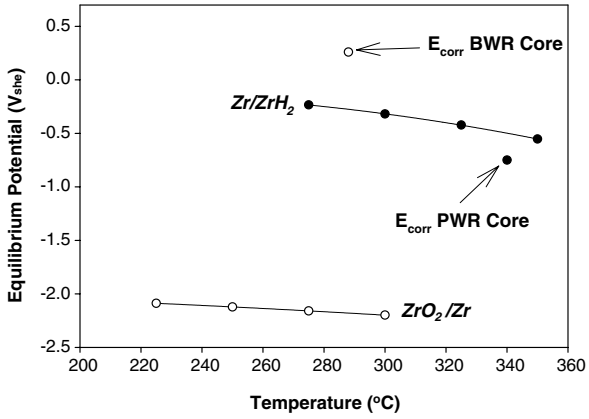

Fig. 1. Comparison of the electrochemical conditions that exist in the cores of BWRs and PWRs in relationship with the equilibrium potentials for the Zr/ZrH_2 and ZrO_2/Zr reactions. The equilibrium potentials for the PWR core were calculated assuming [B] = 1000 mg/kg and [Li] = 2 mg/kg, while those for the BWR core assumes pure water to be the coolant. The corrosion potentials for the PWR core were taken from Urquidi-Macdonald and Macdonald [51] whereas that for the BWR core was taken from Yeh, Macdonald, and Motta [52]. After Park et al. [36].

formation of the hydride is a reduction process ($Zr + 2H_2O + 2e^- \rightarrow ZrH_2 + 2OH^-$), with the currents being positive and negative, respectively. From Pourbaix's formula, $[(E - E^e)I \geqslant 0)]$, where E is the potential (ECP) and E^e is the equilibrium potential, we see that the formation of ZrO_2 as the barrier layer is spontaneous in the BWR case (because $E > E^e$), whereas the formation of ZrH_2 as the barrier layer is spontaneous in the PWR case (because $E < E^e$). Of course, this argument is couched in terms of the stoichiometric phases and the exact identity of the hydride phase remains uncertain, but the differences in the ECP and the equilibrium potentials are sufficiently large (Fig. 1) that it is unlikely that non-stoichiometry alone could change the Gibbs energies of formation to the extent necessary to alter these conclusions. That the thermodynamics are consistent with observation is supported by the micrographs shown in Fig. 2 for highly hydrogenated coolants (conventional PWRs), where the barrier layer is a continuous defective hydride (ZrH_{2-x}) and the outer layer is a precipitated oxide (ZrO_2). Likewise, for oxidizing BWR conditions, the barrier layer is tetragonal ZrO_2, whereas the outer layer is monoclinic ZrO_2, as observed by Ding and Northwood [38] from transmission electron microscopy images and selected-area electron diffraction patterns.

3. Experimental

A controlled hydrodynamic apparatus that was previously developed [39] for performing electrochemical and corrosion studies in high-temperature aqueous systems was used to carry out all electrochemical experiments in this study (Fig. 3). The three-electrode test cell comprised a 600 mL reactor containing a magnetically activated impeller, a thermocouple, a working electrode, a counter electrode,

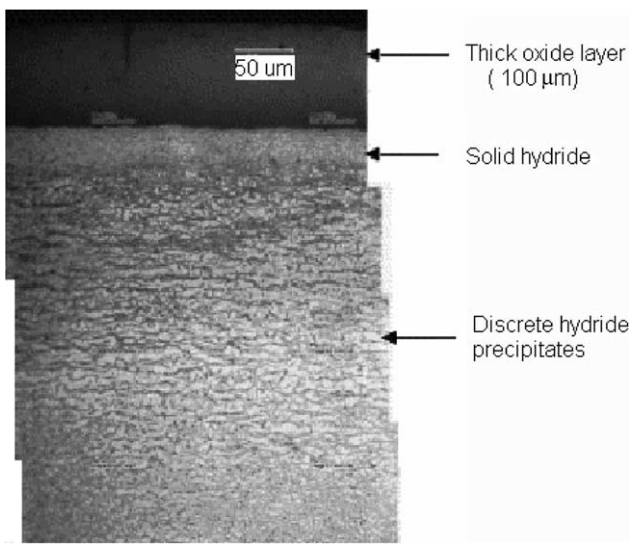

Fig. 2. A continuous hydride barrier layer and discrete hydride precipitates in a Zircaloy-4 cladding tube (average fuel burn-up of 67 GWd/t and fast neutron fluence of 1.3×10^{22} n/cm^2) (Courtesy of R. Daum, Argonne National Laboratory).

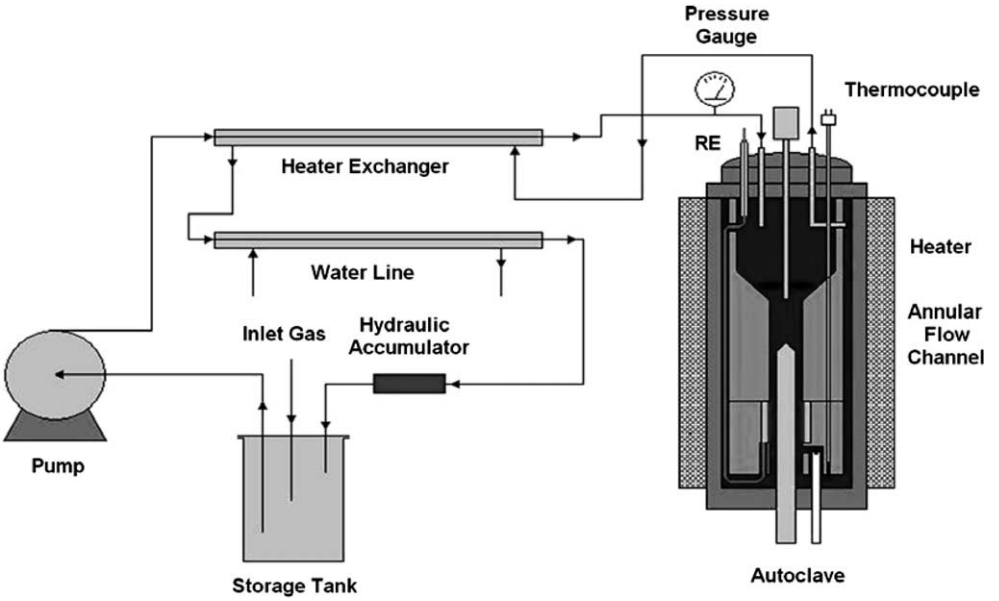

Fig. 3. Schematic of the once-through/recirculating flow loop and the controlled hydrodynamic, high-temperature/high-pressure test cell.

a reference electrode, and an annular flow channel. The working electrode was fabricated from polycrystalline zirconium (99.2%) rod from Alfa Acer with an exposed surface area of 5.82 cm^2. Zirconium rod used in this study contains 0.25 wt% Sn, 0.01 wt% Ni, 0.11 wt% Fe, and 0.01 wt% Cr, determined by electron probe micro analysis (EPMA). The sample was abraded with 800 and 1200 grit SiC paper, and then further polished with 3 μm and 1 μm diamond paste one day before the experiment. An insulated Type 316 L SS wire was connected to the bottom of the annular flow channel by a small screw and then taken out through the top of the vessel via an insulated pressure fitting, with the whole channel serving as the counter electrode. The flow channel was also used to direct the flowing solution over the specimen and to establish well-developed hydrodynamic and mass transport regimes. Previous studies on an identical channel demonstrated that linear flow velocities of several meters per second could be achieved at 300 °C [39].

Two kinds of reference electrodes were used in this study; a Ag/AgCl (sat. KCl) electrode and a Pt/H_2 electrode for use in non-hydrogenated and hydrogenated environments, respectively. The Ag/AgCl (sat. KCl) reference electrode comprised a silver rod that had been anodically plated with silver chloride in a 0.1 M HCl solution at a current density of 5 mA/cm^2 for 18 h. The Ag/AgCl rod was housed in a PTFE tube fitted with a porous zirconia plug at one end with the silver rod protruding through a PTFE cylinder. The inner compartment was filled with KCl crystals and saturated KCl solution with sufficient solid KCl to ensure that the solution remained saturated at all temperatures. The stability of the reference electrode at ambient temperature was checked against a saturated calomel electrode (SCE) before and after the experiments. The porous zirconia liquid junction of the reference electrode was guided to a hole that had been machined from the bottom of the channel to a point just opposite of the specimen (Fig. 3), in order to minimize the uncompensated resistance that would be experienced in the electrochemical studies. For consistency in reporting electrochemical potentials, all measured potentials were converted to the standard hydrogen electrode (SHE) scale by thermodynamic calculation.

To simulate the PWR primary water chemistry, aqueous solutions containing 0.1 M $B(OH)_3$ + 0.001 M LiOH were used. Pressurized water reactors operate with boric acid as a nuclear shim to control the nuclear reactivity. Lithium hydroxide (LiOH) is produced by the nuclear reaction ${}_5B^{10} + {}_0n^1 \rightarrow {}_3Li^7 + {}_2He^4$, but the total lithium concentration is controlled in concert with the boric acid concentration, in order to minimize the release of corrosion products into the coolant and to inhibit their deposition onto the fuel surfaces. Typically, a hydrogen concentration of 25–35 cm^3(STP)/$kg(H_2O)$ (2.2–3.1 ppm H_2) is maintained to inhibit

the formation of radiolytic oxygen in the coolant. All experiments reported here were carried out at 250 °C and a pressure of 62 bar (900 psi) in order to maintain a single liquid phase in the system. The hydrogen content in the solution was adjusted by bubbling ultra-high purity hydrogen gas at an appropriate pressure through the solution in the storage tank overnight at room temperature before the solution was continuously fed into the autoclave. The solutions were prepared from boric acid (Alfa Aesar), lithium hydroxide (Merck), and deionized water (milli-Q system, 18.2 $M\Omega\,cm^{-1}$).

The simulated BWR coolant comprised 0.1 M $B(OH)_3 + 0.001$ M LiOH for pH control, as in the PWR case, but the solution was sparged with argon, rather than with hydrogen. Of course, the coolant in the primary circuit of a BWR is nominally pure water, but electrochemical studies require a significant conductivity in order to control the properties of the system; the required conductivity was provided by the buffer.

Passive films were grown on zirconium potentiostatically. Potential control was achieved by using an electrochemical interface (Solartron Model 1287) in a floating configuration. Potentiodynamic polarization curves were measured using a voltage scan rate of 1 mV/s from a point 0.2 V more negative than the open circuit potential. At each potential step in the potentiostatic film growth studies, the current was monitored as a function of time until steady state was achieved (defined as the current not changing perceptibly over 24 h). Then, the electrochemical impedance was recorded with a Solartron 1255B Frequency Response Analyzer using an excitation voltage of 10 mV (peak-to-peak) and an applied frequency from 100 kHz to 0.01 Hz. All EIS data were measured in the ascending voltage direction. The capacitance was measured using an excitation voltage of 10 mV (peak-to-peak) at a high frequency of 15 kHz.

4. Results and discussion

The passive films formed anodically on zirconium in the 0.1 M $B(OH)_3 + 0.001$ M LiOH solution at 250 °C and 62 bar (900 psi) display golden, blue, purple, or black colors, depending on the formation potential and exposure time. All the films formed on the samples, polished to 1 μm finish, were shiny and smooth while localized corrosion was noticed on the unpolished sample surface as shown in Fig. 4. All electrochemical experiments reported below were carried out on polished samples.

4.1. Polarization studies

The logarithm of the current was recorded as a function of the electrode potential under potentio-

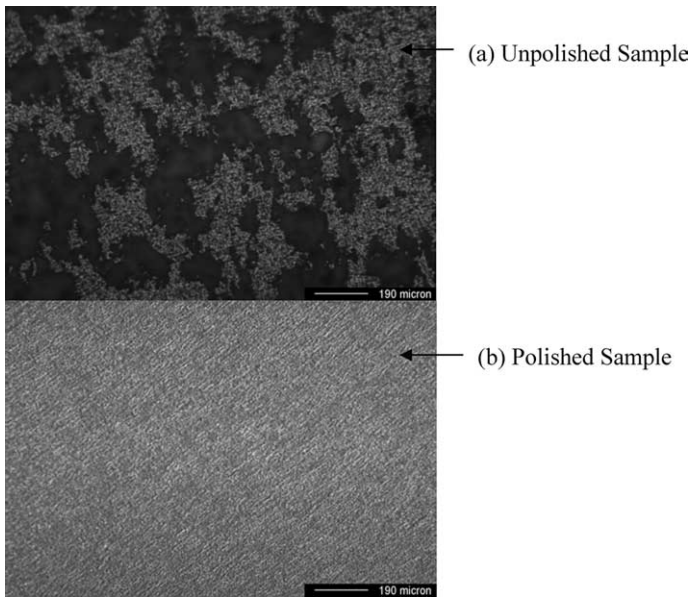

Fig. 4. Examples of localized corrosion on unpolished Zr sample (a) and uniform corrosion on polished Zr sample (b) formed in 0.1 M $B(OH)_3$ and 0.001 M LiOH solution at $T = 250$ °C and $P = 62$ bar.

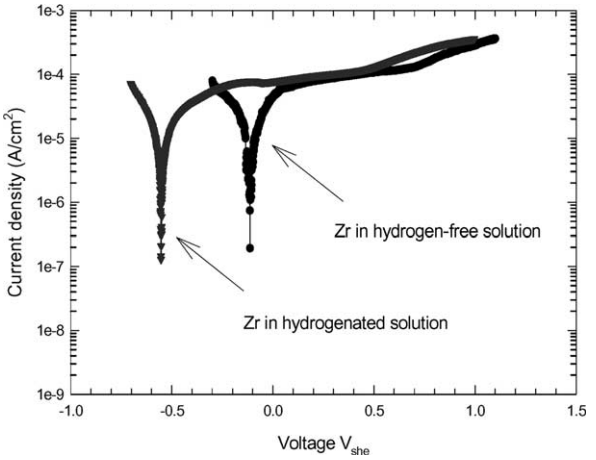

Fig. 5. Comparison of polarization curves for Zr in the hydrogenated and hydrogen-free environments. The electrolyte was 0.1 M $B(OH)_3 + 0.001$ M LiOH, with the solution reservoir at ambient temperature being sparged with high-purity argon gas or hydrogen gas before and during the experiments. For the hydrogen case, 22 cm^3(STP)/kg(H_2O) hydrogen was maintained in the reservoir by suitably controlling the total gas pressure in the system. Scan rate = 1 mV/s, $T = 250$ °C and $P = 62$ bar.

dynamic condition by starting the voltage sweep at a rate 1 mV s^{-1} from a point 0.2 V more negative than the open circuit potential (Fig. 5). For the passive film formed in the solution containing 22 cm^3(STP)/kg(H_2O) hydrogen, passivity dominates the polarization curve from $-0.2\ V_{she}$ to around $0.5\ V_{she}$; at higher potentials, the system exhibits transpassive behavior, as indicated by a steeper rise in the current density. The polarization curve for zirconium in the same solution but without hydrogen displays a much more positive zero current potential with the available passive region extending from $0\ V_{she}$ to $0.7\ V_{she}$. As shown, the zero current potential of zirconium is lowered by more than 0.45 V by the introduction of hydrogen into the solution.

Potentiostatic experiments were carried out by holding the potential at the desired value for film growth until there was no perceptible change in current over 24 h. The logarithm of the stationary current density for the passive film formed on zirconium in hydrogen-free or hydrogenated solution is found to be independent of the formation potential (Fig. 6). The stationary current density is slightly greater for the former than for the latter, indicating that the oxidation of hydrogen contributes little to the observed current. The independence of the logarithm of the current density on the applied potential is consistent with the diagnostic

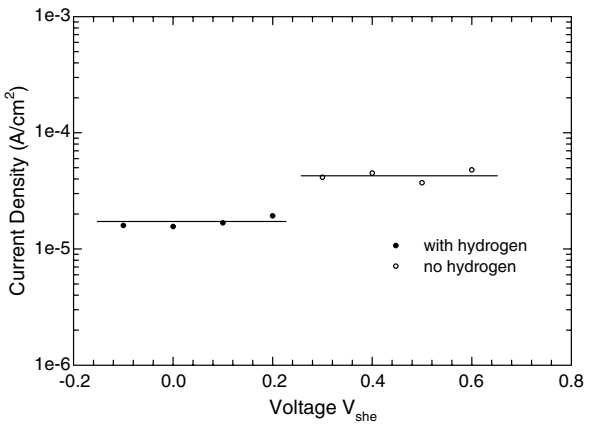

Fig. 6. Steady current density plotted as a function of passive film formation potential. The current was recorded after 24 h stabilization at each potential in the ascending voltage direction. $T = 250$ °C and $P = 62$ bar.

criteria of PDM [35] for an *n*-type passive film. The *n*-type electronic character of the passive film is further demonstrated by the capacitance measurement described later in this paper.

Linear relationships are obtained between the film thickness and the applied potential in the passive regions for both the PWR and BWR cases when the passive films are formed potentiostatically, as shown in Fig. 7. The film thickness was calculated from the capacitance measured at frequencies higher than 1 kHz. At these frequencies, the electrochemical impedance displays an almost purely capacitive frequency response, as shown in Fig. 8,

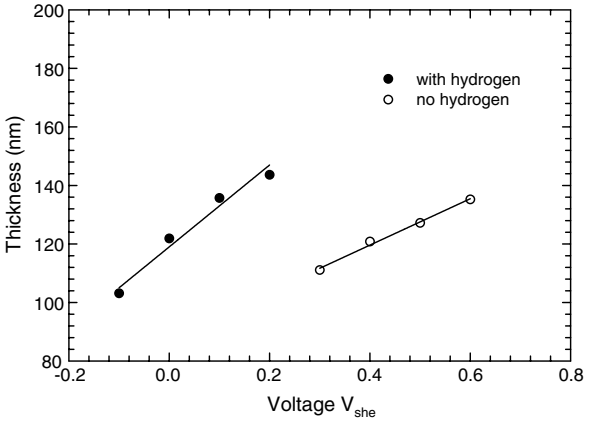

Fig. 7. Dependence of the zirconium passive film thickness on applied potential in 0.1 M $B(OH)_3 + 0.001$ M LiOH solution with or without hydrogen. The potential was changed in the negative-to-positive direction. The film thickness was measured after holding potential at each step for 24 h for film stabilization. $T = 250$ °C and $P = 62$ bar.

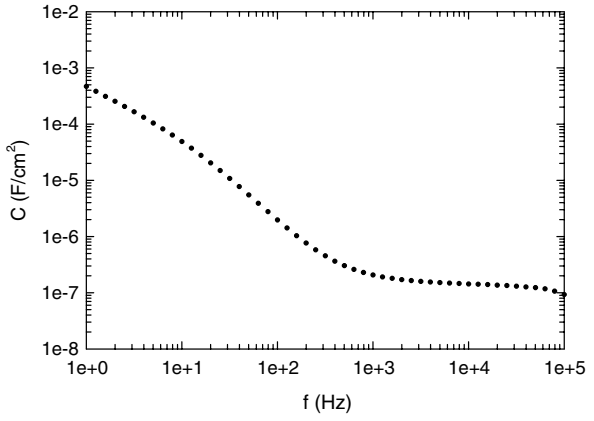

Fig. 8. Measured capacitance as a function of frequency for passive zirconium after holding the potential constant at 0.6 V_{she} for 24 h for film formation in 0.1 M $B(OH)_3 + 0.001$ M LiOH solution. The capacitance is almost independent of frequency for $f > 1$ kHz.

with the measured capacitance being almost independent of frequency. Accordingly, the well-known 'parallel plate' expression for the capacitance is used to estimate the steady state film thickness, L_{ss}

$$L_{ss} = \frac{\varepsilon\varepsilon_0}{C}, \tag{10}$$

where ε_0 is the vacuum permittivity (8.85×10^{-14} F/cm) and $\varepsilon = 22$ [26] is the dielectric constant of the passive film (ε is quoted [21] as being 20–31.5 for ZrO_2. Same value is assumed for the passive film formed in the hydrogenated environment as it comprises a thick ZrO_2 outer layer over a thin ZrH_{2-x} barrier layer). The film thickness calculated from the measured capacitance (Fig. 7) is found to be a linear function of the applied potential. The anodizing constants are 121 nm/V for the passive film formed on zirconium in the hydrogenated solution and 79 nm/V for that formed in the solution without hydrogen. These values are much greater than the 1.9–2.5 nm/V normally found for barrier layer formed on metals and alloys at ambient or near-ambient temperatures. The higher values are attributed to the formation of thick outer layers over thin barrier layers, as previously shown for the passive film formed on zirconium in 1 M H_3PO_4 [40] at ambient temperature. Accordingly, the measured capacitance, which may be represented as a series combination of the two layers, is dominated by the outer layer, as shown by the following equation

$$\frac{1}{C} = \frac{1}{\varepsilon_0}\left[\frac{L_{bl}}{\varepsilon_{bl}} + \frac{L_{ol}}{\varepsilon_{ol}}\right]. \tag{11}$$

Here L_{bl} is the thickness of barrier layer and L_{ol} is the thickness of outer layer. Thus, noting that the dielectric constants for the barrier layer and the outer layer are probably of similar magnitude (this is certainly the case for BWR conditions, where both layers comprise ZrO_2), then for $L_{ol} \gg L_{bl}$ the measured capacitance is dominated by the outer layer. Since the outer layers in both environments are porous ZrO_2, the data plotted in Fig. 7 indicate that the outer layer is significantly thicker when formed in the hydrogenated solution than when grown in the hydrogen-free solution. This finding also accounts for the difference in the passive current density, also shown in Fig. 6, because of the expected impact of the outer layer on the interfacial impedance. Finally, Eq. (11) should be regarded as being a first approximation, because the barrier layer also possesses semiconductor properties that can be interpreted in terms of Mott–Schottky theory (see below). This first approximation is valid, because the outer layer dominates the capacitance.

4.2. Electrochemical impedance spectroscopy

Electrochemical impedance spectra (EIS) for passive zirconium films were measured over a wide range of frequencies (typically 100 kHz to 0.01 Hz) as a function of formation potential across the passive range in solutions with and without hydrogen at 250 °C. The impedance was measured after holding the potential constant at each point for 24 h, in order to ensure that the passive film exists in the steady state. The measurements were carried out in the ascending potential direction. Since the stability of the electrochemical system during EIS measurement is critical to obtaining viable data, the quality of the EIS data was checked both experimentally and theoretically. The data were checked experimentally by stepping the frequencies from high-to-low and then immediately back from low-to-high, with the impedance being measured at each step, to ascertain that the same values were obtained at equivalent frequencies in the two directions. If the system is in the steady state, which means the thickness and current are independent of time, the impedance data should match in the two potential step directions. The Nyquist and Bode plots (Fig. 9) show that the impedance data measured in the two step directions after holding the potential at 0.1 V_{she} for 24 h for the film to attain a steady state are coincident. Coincidence is observed in all impedance measurements for passive films formed in hydrogenated solution

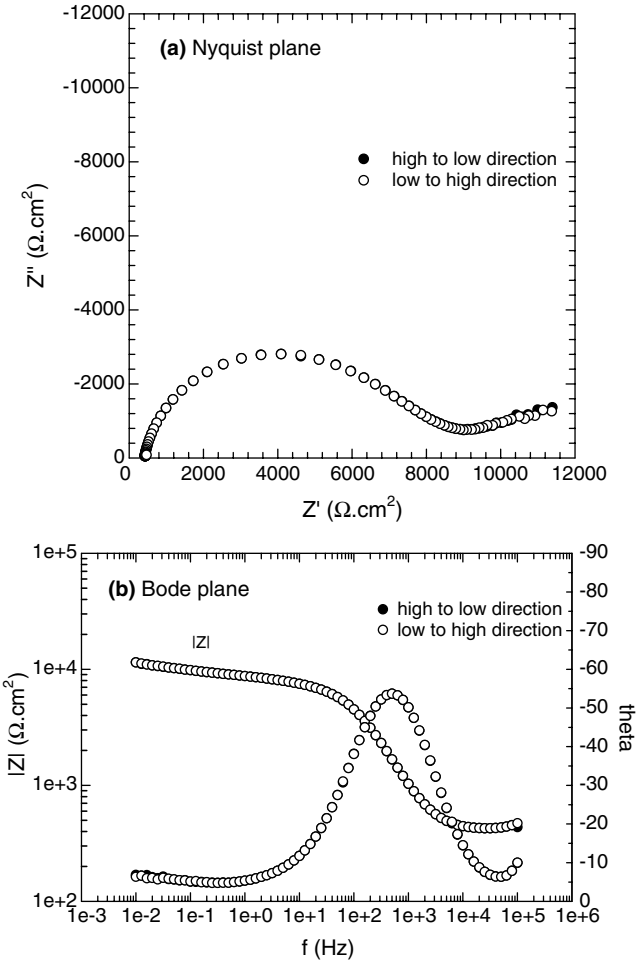

Fig. 9. Comparison of Nyquist (a) and Bode (b) plots for passive zirconium formed at 0.1 V_{she} for 24 h by scanning the frequency in the high-to-low direction and immediately from the low-to-high direction in 0.1 M $B(OH)_3$ + 0.001 M LiOH solution with 22 cm^3(STP)/kg(H_2O) hydrogen. $T = 250$ °C and $P = 62$ bar. 'High-to-low' means stepping the frequency from high to low direction and 'low-to-high' means stepping the frequency in the reverse direction.

and hydrogen-free solution at different potentials. This is a particularly good test for system stability.

The quality of the impedance data was also checked using the Kramers–Kronig transforms. These integral transforms test for compliance of the system with the linearity, stability, and causality constraints of linear systems theory (LST). The K–K transforms, which arise from Cauchy's theorem and the definition of causality, were first developed for the field of optics by establishing a connection between the real and imaginary parts of complex optical parameters (e.g., refractive index). The K–K transforms are purely mathematical results and do not reflect any assumptions concerning the physical properties of the system. Thus, only the experimental data satisfying the linearity, stability, and causality constraints, as indicated by the K–K transforms, can be used to describe the properties of the systems in terms of linear response theory. Macdonald and Urquidi-Macdonald [41–45] developed methods for transforming the real part of the electrochemical impedance into the imaginary part of the impedance and vice versa. Their studies show that the K–K transforms are strongly sensitive to the violation of the stability constraint, but are not particularly sensitive to violation of the linearity condition. Fig. 10 shows a set of K–K transforms, in which the transformed components of the impedance are compared with the corresponding measured components. Excellent agreement is obtained, except for the small discrepancies at low frequencies; the discrepancies are due to the 'tails'

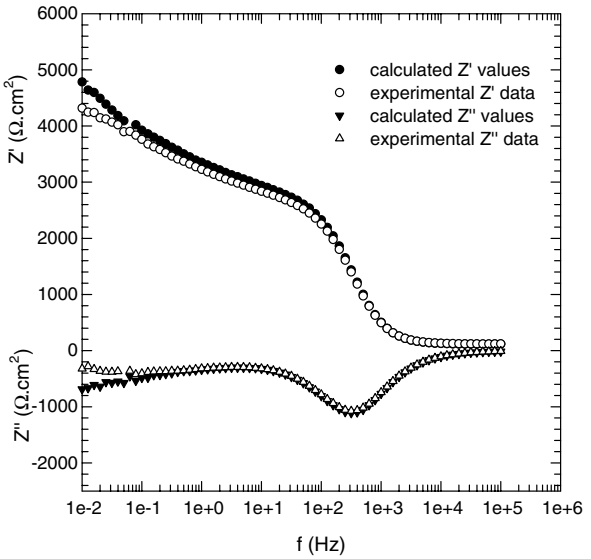

Fig. 10. Typical Kramers–Kronig transforms of the real and imaginary components of the impedance of passive zirconium in 0.1 M $B(OH)_3 + 0.001$ M LiOH solution at $T = 250$ °C and $P = 62$ bar. The oxide film was formed at 0.6 V_{she}. 'Calculated' real and imaginary components were derived from the experimental imaginary and real components, respectively, by using the K–K transforms. These data are compared with the experimental real and imaginary components of the impedance, respectively.

problem that arises from the fact that the impedance data are measured over a finite bandwidth whereas the transforms are defined over an infinite bandwidth in frequency.

Fig. 11(a) and (b) shows Nyquist and Bode plots for zirconium at various potentials in the passive range in the 0.1 M $B(OH)_3 + 0.001$ M LiOH solution with argon or with hydrogen gas at 250 °C and 62 bar. The magnitude of the impedance of the passive film formed in the presence of hydrogen is much higher than that formed without hydrogen, in good correlation with the passive current behavior and the film thickness data discussed above. In terms of point defect model, the higher impedance of the interface exposed to hydrogenated solutions can be attributed to a thicker outer layer, which probably results from a higher rate of formation than in the BWR case. Thus, for PWR environments, the thermodynamic data are consistent with the barrier layer being a defective hydride, possibly ZrH_{2-x}. It is likely that the defect is exclusively the hydrogen vacancy, so that formation of the outer layer will occur by hydrolysis of the hydride, rather than via restructuring of the outer surface of the barrier layer or the hydrolysis/precipitation of cations transmitted through the barrier layer, as in the simulated BWR case. This reaction

$$ZrH_2(\text{barrier layer}) + 2H_2O \rightarrow ZrO_2(\text{porous outer layer}) + 3H_2 \quad (12)$$

is likely to be fast compared with the corresponding reaction for the BWR case

$$\left.\begin{array}{l} ZrO_2(\text{barrier layer}) \rightarrow ZrO_2(\text{porous outer layer}) \\ \text{or} \quad Zr^{4+} + 2H_2O \rightarrow ZrO_2(\text{porous outer layer}) + 4H^+ \end{array}\right\}. \quad (13)$$

Since the rates of dissolution of the outer layers in both cases are likely to be similar, the higher rate of Reaction (12) compared with Reaction (13) should lead to a thicker, more resistive film in the PWR case than in the BWR case, as observed.

The shapes of the Nyquist plots for zirconium in the solutions with and without hydrogen are virtually the same, both showing depressed semicircles at high frequencies and a Warburg tail of constant phase angle of 4–8° according to Fig. 11 at low frequencies ($f < 1$ Hz). The impedance is insensitive to film formation potential within the passive range. In terms of the postulates of the PDM, the electric field strength is independent of the formation potential, and the transport of the defects is driven by the electric field strength. Therefore, the impedance should be insensitive to the film formation potential as has been observed for other systems [46]. However, as argued above, the impedance is dominated by the properties of the outer layer and it is unlikely that the barrier layer makes a significant contribution other than being the sources of outer layer material, as described by Reactions (12) and (13).

4.3. Mott–Schottky analysis

An understanding of the crystallographic and electronic defect structures of the passive film on zirconium is vital in exploring the underlying mechanisms of oxidation and hydriding of Zircaloy fuel cladding in reactor coolant environments. To identify the principal defect in the passive film, Mott–Schottky (M–S) analysis [34] is being used. In M–S analysis, the capacitance of passive Zr is measured at a suitably high frequency as a function of voltage. According to Mott–Schottky theory [47], the space charge capacitances, C_{sc} (F/cm^2), of n-type and p-type semiconductor junctions are given by

$$\frac{1}{C_{sc}^2} = \frac{2}{\varepsilon\varepsilon_0 q N_D}\left(V - V_{fb} - \frac{kT}{q}\right) \quad n\text{-type} \quad (14)$$

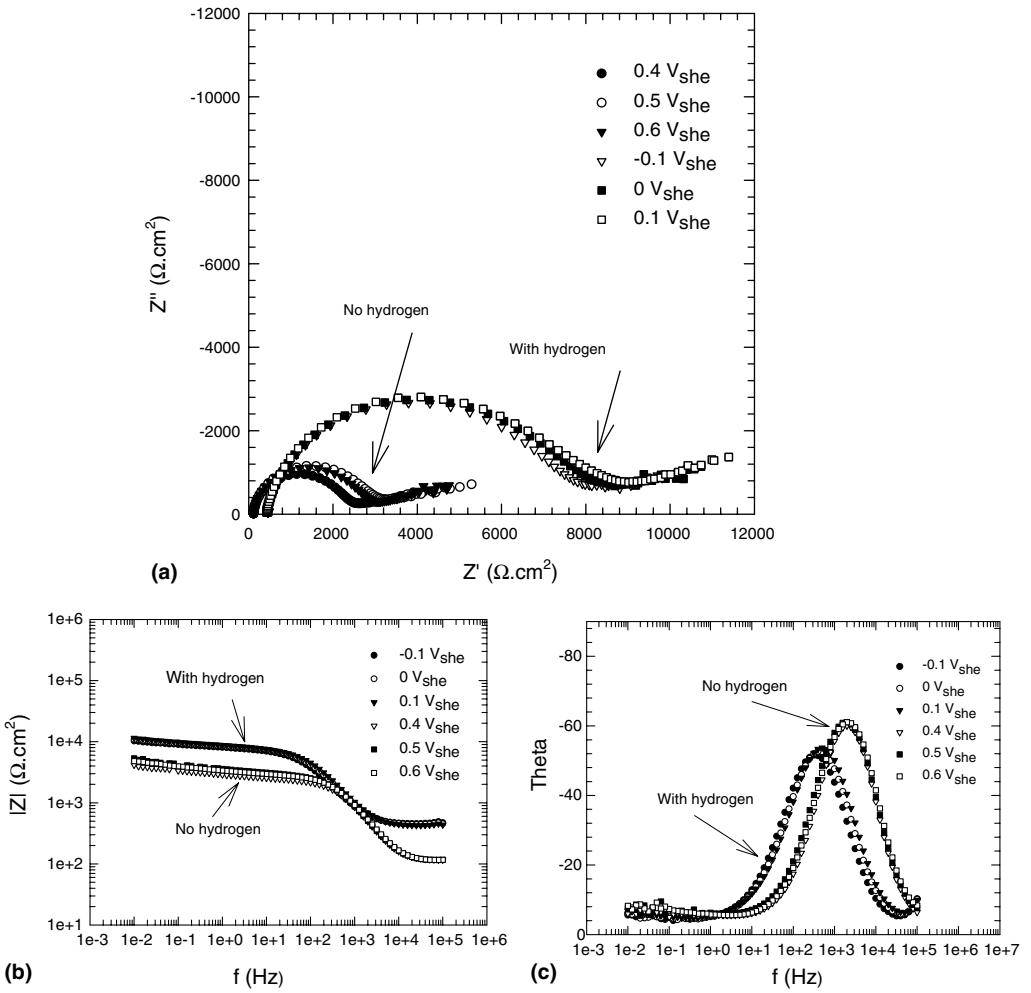

Fig. 11. Impedance spectra for passive zirconium as a function of film formation potential in 0.1 M $B(OH)_3 + 0.001$ M LiOH solutions with and without added hydrogen. The impedance was measured after holding the potential at each step for 24 h for film stabilization. The potentials was changed in the negative-to-positive direction. $T = 250$ °C and $P = 62$ bar.

and

$$\frac{1}{C_{sc}^2} = \frac{-2}{\varepsilon\varepsilon_0 q N_A}\left(V - V_{fb} - \frac{kT}{q}\right) \quad p\text{-type} \tag{15}$$

respectively. In these expressions, N_D/N_A is the donor/acceptor concentration (cm^{-3}), ε_0 is the vacuum permittivity (8.85×10^{-14} F/cm), ε is the dielectric constant of the oxide, V is the applied potential, V_{fb} is the flat band potential, q is the electron charge (1.6×10^{-19} C), and kT/q is about 45 mV at 250 °C. In addition to confirming the electronic nature of the film, M–S analysis yields the dopant concentration (donor or acceptor) in the film as a function of voltage. The interfacial capacitance C is obtained from $C = -1/\omega Z''$.

Assuming that the capacitance of the Helmholtz layer can be neglected, the measured capacitance C is equal to the 'space charge' capacitance, C_{sc}. Accordingly, a C_{sc}^{-2} versus V plot should be a straight line with a slope that is inversely proportional to the dopant concentration.

The outer layer of the passive film formed on zirconium is found to be much thicker than the barrier layer. The thin barrier layer is a defective phase with semiconductor properties that depend upon the type of defects present while the outer layer is relatively porous and has no appreciable semiconductor properties [48]. Therefore, the measured capacitance cannot be directly approximated as the space charge capacitance; instead, the observed capacitance C

can be understood by postulating that it reflects a series combination of a voltage-independent capacitance, C_{ox}, due to the outer layer insulting layer, and the space charge capacitance, C_{bl}, of the barrier layer, as discussed in the thickness calculation section of this paper.

$$\frac{1}{C} = \frac{1}{C_{ox}} + \frac{1}{C_{bl}}. \tag{16}$$

It has been shown by de Gryse et al. [49] that the measured capacitance can be related to C_{ox} and the applied voltage by

$$\frac{1}{C^2} = \frac{1}{C_{ox}^2} + \frac{2}{\varepsilon\varepsilon_0 q N_D}\left(V - V_{fb} - \frac{kT}{q}\right). \tag{17}$$

where the notation is same as previously defined. As can be seen from this expression, the slope of the MS-plot is not influenced by the oxide capacitance C_{ox} and can be used to derive reliable values for the donor density, N_D, from the slope of the measured MS-plot, although the intercept is shifted on the vertical and horizontal axes, thereby yielding a flat band potential that is too negative. Mott–Schottky analysis can be applied to a system of fixed (voltage-independent) total dopant concentration and, hence, C versus V must be measured under the conditions that do not result in a change in the dopant concentration profile of the film. In this work, after holding the specimen at the desired potential for 24 h, in order for the film to reach steady state, the capacitance was recorded while simultaneously sweeping the voltage in the negative direction from the formation potential at a sweep rate of 25 mV/s. This sweep rate is considered to be sufficiently high that the defect structure is 'frozen-in' and hence that N_D in Eq. (17) appears as a constant (identical M–S slopes were obtained for different scan rates over 25 mV/s, as shown in Fig. 12). Mott–Schottky plots are presented in Fig. 13 and Fig. 14 for passive Zr formed in hydrogenated and hydrogen-free solutions at different formation potentials. From the positive slopes, it is concluded that the passive films on zirconium formed in high temperature borate buffer solutions with or without hydrogen exhibits *n*-type electronic character. This result shows that the dominant defects in the film over this voltage range are oxygen/hydrogen vacancies and/or zirconium interstitials. The donor density N_D versus the formation potential (Fig. 15) has been calculated from the slopes in Figs. 13 and 14 for passive films formed in hydrogenated and hydrogen-free solutions. The data show that

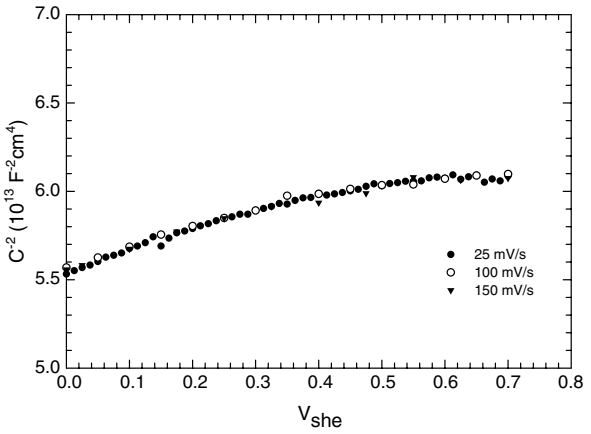

Fig. 12. Mott–Schottky plots for passive Zr formed at 0.7 V_{she} in 0.1 M $B(OH)_3$ + 0.001 M LiOH solution without hydrogen in the reservoir, measured at different scan rates. $T = 250$ °C and $P = 62$ bar. Identical slopes were found for scan rate $\geqslant$ 25 mV/s.

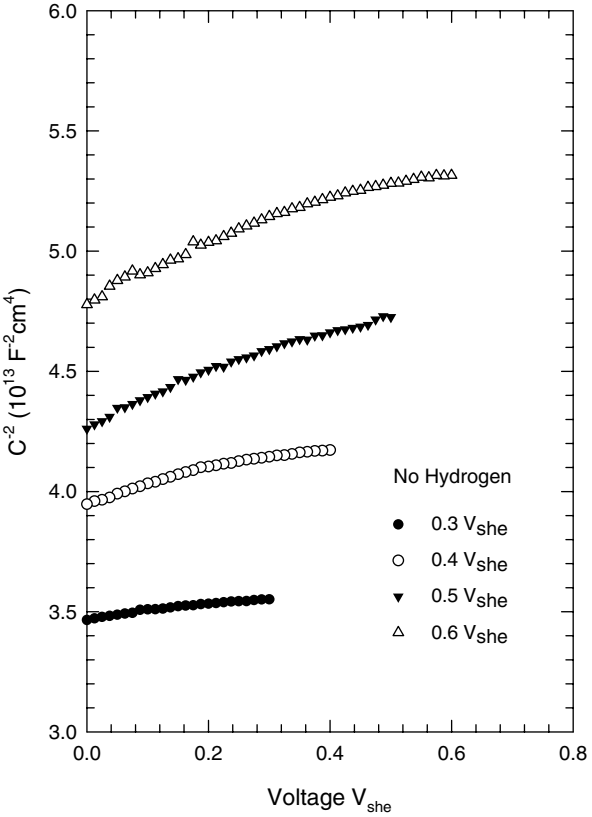

Fig. 13. Mott–Schottky plots for the Zr passive film formed at the indicated potentials after stabilization for 24 h in 0.1 M $B(OH)_3$ + 0.001 M LiOH solution sparged with argon gas. Voltage sweep rate in the negative direction from the formation voltage = 25 mV/s. $T = 250$ °C and $P = 62$ bar.

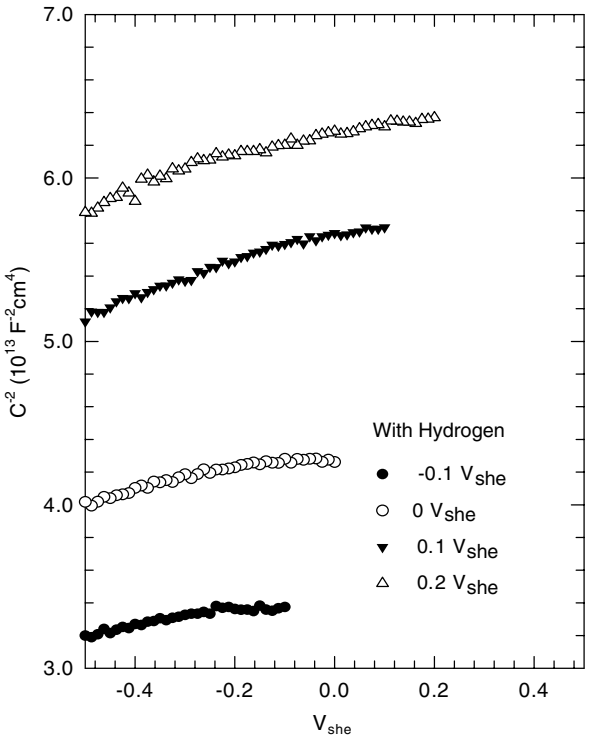

Fig. 14. Mott–Schottky plots for passive Zr at the indicated potentials after stabilization for 24 h in 0.1 M $B(OH)_3 + 0.001$ M LiOH solution with 22 cm^3(STP)/kg(H_2O) hydrogen. Voltage sweep rate in the negative direction from the formation voltage = 25 mV/s. $T = 250$ °C and $P = 62$ bar.

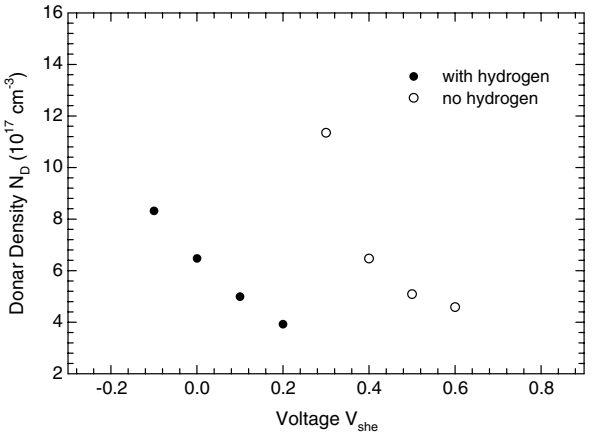

Fig. 15. Donor density N_D of the passive film formed on Zr as a function of film formation potential in 0.1 M $B(OH)_3 + 0.001$ M LiOH solutions with or without hydrogen. $T = 250$ °C and $P = 62$ bar.

the donor concentration in the vicinity of the metal/film interface decreases with increasing formation potential for both cases, in agreement with the prediction of the point defect model [35]. The donor concentration, N_D, is in the range of 10^{17}–10^{18} cm^{-3}, which agrees with the $N_D < 10^{19}$ cm^{-3} reported by Meisterjahn [50] for the zirconium passive film formed at ambient temperature. The much lower donor concentration found here demonstrates that the film is only lowly-doped with electron donors. However, the low doping level probably reflects a composite value for a highly doped, but thin, barrier layer and a thick stoichiometric outer layer.

5. Summary and conclusions

The electrochemistry of zirconium has been explored in situ in 0.1 M $B(OH)_3 + 0.001$ M LiOH aqueous solution (pH = 6.94 at 250 °C) with and without added hydrogen to simulate the water chemistries of the coolant circuits in pressurized water reactors (PWRs) and boiling water reactors (BWRs), respectively. Potentiostatic polarization, potentiodynamic polarization, and electrochemical impedance spectroscopy (EIS) were used, with the latter also being employed for determining the passive film thickness and for carrying out Mott–Schottky analyses. The principal findings and conclusions of this work are as follows:

1. From thermodynamic analysis, it is postulated that a hydride barrier layer forms under PWR coolant conditions, whereas an oxide barrier layer forms under BWR primary coolant conditions. Thus, the introduction of hydrogen into the solution lowers the corrosion potential of zirconium to the extent that the formation of ZrH_2 is predicted to be spontaneous rather than the ZrO_2.
2. The logarithm of the steady state passive current density is found to be independent of formation potential, while the steady-state film thickness (L_{ss}) is a linear function of the formation potential. The much greater anodizing constants $(\partial L_{ss}/\partial V)_{pH}$ than for other metals and alloys at ambient temperature suggest that a thick outer layer forms over a thin barrier layer.
3. The Nyquist plots of the impedance are in the form of depressed semicircles with a Warburg like impedance at low frequencies for both the PWR and BWR cases. The magnitude of impedance of the passive film formed in the hydrogenated solution is much higher than that for the film formed in the hydrogen free solution, which is consistent with the measured passive currents for the two cases.

4. Mott–Schottky analysis shows that the passive film formed anodically on zirconium under BWR- and PWR-like environments is *n*-type in electronic character, corresponding to a preponderance of oxygen/hydrogen vacancies and/or zirconium interstitials, with the former being likely, in the barrier layer.
5. The *n*-type electronic character of the film is consistent with the diagnostic criteria offered by point defect model.
6. The donor concentration is in the range of 10^{17}–$10^{18}\,cm^{-3}$, which decreases with increasing formation potential, demonstrating that the film is only lowly-doped with electron donors. However, the low doping level probably reflects a composite value for a highly doped, but thin, barrier layer and a thick, stoichiometric outer layer.

Acknowledgements

The authors gratefully acknowledge the support of this work by the Department of Energy's Nuclear Energy Research Initiative (NERI) under Grant DE-FG07-02SF22618.

References

[1] R.B. Adamson, L.F.P. Van Swam (Eds.), Zirconium in the Nuclear Industry: Seventh International Symposium, ASTM, Philadelphia, PA, 1987.
[2] ASM Handbook, Vol. 13, Corrosion, ASM International, Materials Park, OH, 1990.
[3] Corrosion of Zirconium Alloys in Nuclear Power Plants, IAEA-TECDOC-684, IAEA, Vienna, 1993.
[4] B. Cox, J. Nucl. Mater. 170 (1990) 1.
[5] ICONE8, Proceedings of the 8th International Conference on Nuclear Engineering, American Society of Mechanical Engineers, New York, 2000.
[6] ICONE10, Proceedings of the 10th International Conference on Nuclear Engineering, American Society of Mechanical Engineers, New York, 2002.
[7] ICONE12, Proceedings of the 12th International Conference on Nuclear Engineering, American Society of Mechanical Engineers, New York, 2004.
[8] D.L. Douglass, The Metallurgy of Zirconium, International Atomic Energy Agency, Vienna, 1971.
[9] C.M. Eucken, A.M. Garde (Eds.), Zirconium in the Nuclear Industry: Ninth International Symposium, American Association for Testing and Materials, Philadelphia, PA, 1991.
[10] A.M. Garde, E.R. Bradley (Eds), Zirconium in the Nuclear Industry: Tenth International Symposium, ASTM Special Technical Publication, Vol. 1245, Philadelphia, PA, 1994.
[11] D.G. Franklin, R.B. Adamson (Eds), Zirconium in the Nuclear Industry: Sixth International Symposium. ASTM Special Technical Publication, Vol. 824, Philadelphia, PA, 1984.
[12] A. Goossens, M. Vazquez, D.D. Macdonald, Electrochim. Acta 41 (1996) 47.
[13] P. Greenfield, Zirconium in Nuclear Technology, Mills and Boon, London, 1972.
[14] B. Lustman, F. Kerze, The Metallurgy of Zirconium, First Ed., McGraw-Hill, New York, 1955.
[15] G.L. Miller, Zirconium, 2nd Ed., Butterworths Scientific Publications, London, 1957.
[16] G.D. Moan, P. Rudling (Eds.), Zirconium in the Nuclear Industry: Thirteenth International Symposium, ASTM, West Conshohocken, PA, 2002.
[17] G.P. Sabol, G.D. Moan (Eds.), Zirconium in the Nuclear Industry: Twelfth International Symposium, ASTM, West Conshohocken, Pennsylvania, 2000.
[18] G.P. Sabol, E.R. Bradley (Eds.), Zirconium in the Nuclear Industry: Eleventh International Symposium, ASTM, West Conshohocken, PA, 1996.
[19] L.F.P. Van Swam, C.M. Eucken (Eds.), Zirconium in the Nuclear Industry: Eighth International Symposium, ASTM, Philadelphia, PA, 1989.
[20] A. Gunterschultze, H. Betz, Z. Elektrochem. 37 (1931) 726.
[21] Waterside Corrosion of Zirconium Alloys in Nuclear Power Plants, IAEA-TECDOC-996, IAEA, Vienna, 1998.
[22] W.M. Small, J.H. Root, D. Khatamian, J. Nucl. Mater. 256 (1998) 102.
[23] J.H. Root, W.M. Small, D. Khatamian, O.T. Woo, Acta Mater. 51 (2003) 2041.
[24] A. Yilmazbayhan, A.T. Motta, R.J. Comstock, G.P. Sabol, B. Lai, Z.H. Cai, J. Nucl. Mater. 324 (2004) 6.
[25] O.N. Pierron, D.A. Koss, A.T. Motta, K.S. Chan, J. Nucl. Mater. 322 (2003) 1.
[26] B. Cox, F. Gascoin, Y.M. Wong, J. Nucl. Mater. 218 (1995) 113.
[27] L. Durand-Keklikian, G. Cragnolino, D.D. Macdonald, Corros. Sci. 32 (1991) 347.
[28] L. Durand-Keklikian, G. Cragnolino, D.D. Macdonald, Corros. Sci. 32 (1991) 361.
[29] S. Hettiarachchi, M.E. Indig, D. Cubicciotti, Electrochemical characteristics of Zircaloys in high temperature aqueous environments, in: Sixth International Symposium on Environmental Degradation of Materials in Nuclear Power Systems – water reactors, 1993.
[30] J. Schefold, D. Lincot, A. Ambard, O. Kerrec, J. Electrochem. Soc. 150 (2003) B451.
[31] G. Nagy, Z. Kerner, G. Battistig, A. Pinter-Csordas, J. Balogh, T. Pajkossy, J. Nucl. Mater. 297 (2001) 62.
[32] G. Nagy, Z. Kerner, T. Pajkossy, J. Nucl. Mater. 300 (2002) 230.
[33] G. Nagy, R. Schiller, Phys. Chem. Chem. Phys. 4 (2002) 791.
[34] D.D. Macdonald, J. Electrochem. Soc. 139 (1992) 3434.
[35] D.D. Macdonald, Pure Appl. Chem. 71 (1999) 951.
[36] P.Y. Park, M.U. Macdonald, D.D. Macdonald, Application of the point defect model (PDM) to the oxidation of zircaloy fuel cladding in water-cooled nuclear reactors, in: ICONE 12, 2004, p. 605.
[37] HSC software, Chemical Reaction and Equilibrium Thermodynamics, SGE International Pty. Ltd.
[38] Y.Q. Ding, D.O. Northwood, Mater. Charact. 30 (1993) 13.
[39] D.D. Macdonald, J. Mankowski, M. Karaminezhaadranjbar, Y.H. Hu, Corrosion 44 (1988) 186.

[40] A. Goossens, M. Vazquez, D.D. Macdonald, Electrochim. Acta 41 (1996) 35.
[41] D.D. Macdonald, M. Urquidi-Macdonald, S. Real, J. Electrochem. Soc. 134 (1987) C419.
[42] D.D. Macdonald, M. Urquidi-Macdonald, J. Electrochem. Soc. 137 (1990) 515.
[43] M. Urquidi-Macdonald, S. Real, D.D. Macdonald, J. Electrochem. Soc. 133 (1986) 2018.
[44] M. Urquidi-Macdonald, S. Real, D.D. Macdonald, Electrochim. Acta 35 (1990) 1559.
[45] M. Urquidi-Macdonald, S. Real, D.D. Macdonald, J. Electrochem. Soc. 133 (1986) C132.
[46] E. Sikora, D.D. Macdonald, Electrochim. Acta 48 (2002) 69.
[47] S. Sze, The Physics of Semiconductor Devices, 2nd Ed., Wiley & Sons, NY, 1981.
[48] P. Park, MS Thesis, The Application of the PDM (Point Defect Model) to the Oxidation of Zircaloy Fuel Cladding in Water-Cooled Nuclear Reactors, in: Department of Engineering Science and Mechanics, Pennsylvania State University, 2004.
[49] R.D. Gryse, W.P. Gomes, F. Cardon, V. Vennik, J. Electrochem. Soc. 122 (1975) 711.
[50] P. Meisterjahn, H.W. Hoppe, J.W. Schultze, J. Electroanal. Chem. 217 (1987) 159.
[51] M. Urquidi-Macdonald, D.D. Macdonald, to be published.
[52] T.K. Yeh, D.D. Macdonald, A.T. Motta, Nucl. Sci. Eng. 121 (1995) 68.